Invasion into the bladder wall generates solitary subpopulations of uropathogenic *Escherichia coli* that are protected from killing by antibiotics and neutrophil swarms in an organoid model

Authors: Kunal Sharma[1], Vivek V. Thacker[1*#], Neeraj Dhar[1*#], François Signorino-Gelo[1], Maria Clapés Cabrer[1], Anaëlle Dubois[1], Jasper Mullenders[2], Graham Knott[1], Hans Clevers[2], John D. McKinney[1*]

Affiliations:

[1]School of Life Sciences, Swiss Federal Institute of Technology in Lausanne (EPFL), 1015 Lausanne, Switzerland.

[2]Oncode Institute, Hubrecht Institute, Royal Netherlands Academy of Arts and Sciences and University Medical Center, Utrecht, Netherlands.

*Correspondence to: vivekvthacker@gmail.com, neeraj.dhar@epfl.ch, john.mckinney@epfl.ch

[#] These authors contributed equally

Abstract:

Uropathogenic *Escherichia coli* (UPEC) is the most common cause of urinary tract infections (UTIs) and require antibiotic therapy. Recurrent infection, which occurs in 25% of treated individuals, is thought to be caused by the release of bacteria from persistent intracellular bacterial communities (IBCs) in the outermost layer of umbrella cells in the bladder wall. Here, we present a bladder organoid model of UPEC infection that recapitulates the bladder architecture within a volume that is suitable for long-term time-lapse imaging of host-pathogen dynamics with high spatiotemporal resolution. We show that bacteria injected into the organoid lumen rapidly invade the bladder epithelium and proliferate intracellularly to form IBCs that are refractory to clearance by antibiotics or neutrophils. Unexpectedly, we find that individual "solitary" bacteria within deeper layers of the organoid wall also resist elimination by antibiotics and neutrophil swarms. Volumetric serial block face scanning electron microscopy of infected organoids reveals that solitary bacteria may be intracellular or pericellular (located between uroepithelial cells). Solitary bacteria are enriched after neutrophil attack and continue to express flagellin (unlike bacteria within the lumen or IBCs, which are flagellin-deficient), suggesting a mechanism for invasion of solitary bacteria into deeper layers of tissue. Through live-cell imaging, we show that solitary bacteria in the organoid wall, that might resemble quiescent reservoirs, are spatially distinct from IBCs but have temporal overlap, indicating that bacterial shedding from IBCs is not the only mechanism for the establishment of solitary bacterial populations in the bladder wall.

Keywords: bladder organoids, uropathogenic *Escherichia coli* (UPEC), intracellular bacterial communities (IBCs), pericellular bacteria, bacterial persistence, antibiotic treatment, neutrophil swarms, live-cell imaging

Introduction:

Urinary tract infections (UTIs) are among the most common bacterial infections and the second most-common cause for the prescription of antibiotics (Foxman, 2010). Although seldom fatal, UTIs substantially reduce the quality of life and incur enormous healthcare costs. Recurrence, defined as a reappearance of infection within 12 months despite the apparently successful completion of antibiotic therapy, occurs in a quarter of all UTIs (Foxman et al., 2000). Women are at particularly high risk, and more than 60% of women will be diagnosed with a UTI at least once in their lifetime (Klein and Hultgren, 2020). Uropathogenic *Escherichia coli* (UPEC) is the causative agent of about 80% of all UTIs, which can be further complicated by dissemination of UPEC from the bladder (cystitis) to the kidneys (nephritis) or into the bloodstream (sepsis).

Much of our current understanding of UPEC pathogenesis has been derived from experiments in mouse models of infection(Hannan and Hunstad, 2016; Hung et al., 2009), which reveal that UPEC can grow extracellularly in the urine within the bladder or intracellularly in the bladder wall(Anderson et al., 2003; Justice et al., 2004; Mulvey et al., 2001). Invasion into the bladder wall is preceded by adherence of UPEC to the superficial umbrella cell layer of the bladder, mediated by interactions of the bacterial type I pilus with uroplakin proteins on the surface of the uroepithelium (Martinez et al., 2000; Mulvey et al., 1998). Following bacterial entry into umbrella cells, a subset of bacteria proliferate to form biofilm-like intracellular bacterial

communities (IBCs) (Anderson et al., 2003; Justice et al., 2004; Mulvey et al., 2000) that may be refractory to clearance by the innate immune system or antibiotic treatment. Additionally, at later stages of infection, UPEC has been shown to penetrate into deeper layers of the bladder to form 'quiescent reservoirs' that may also be responsible for relapse of infection after antibiotic therapy(Mulvey et al., 2000, 2001; Mysorekar and Hultgren, 2006; Schilling et al., 2002). However, these isolated subpopulations are difficult to characterize in bladder sections, and the relative contribution of IBCs and quiescent reservoirs in the persistence of infection remains difficult to document (Blango et al., 2014; Mulvey et al., 2001; Scott et al., 2015). The number of bacteria in these three distinct subpopulations (extracellular bacteria, IBCs, and quiescent reservoirs), their relative growth dynamics, and their persistence under attack from antibiotics or immune cells are difficult to characterize *in situ* using animal models. Most studies therefore rely on an examination of bladder explants at specified time-points post-infection. However, this technique does not provide information on the underlying dynamics of host-pathogen interactions, nor does it permit the quantification of *in situ* growth of extracellular bacteria (Anderson et al., 2003; Justice et al., 2004). *In vitro* models have been developed to probe specific aspects of UPEC infection, such as the role of the stratified bladder architecture (Horsley et al., 2018) or the effects of micturition on IBC formation (Andersen et al., 2012). However, these models suffer from limitations; in their ability to recreate a stratified epithelium with multiple differentiated cell layers (Andersen et al., 2012) or to reproduce the migration of immune cells into the bladder in response to infection (Horsley et al., 2018). In many of these systems, live-cell imaging remains technically challenging (Horsley et al., 2018; Smith et al., 2006).

In the last decade, organoids have emerged as experimentally tractable biomimetics that recapitulate key physiological and functional features of the cognate organs (Clevers, 2016). These complex 3D multicellular structures are generated from stem cells or organ-specific progenitor cells (Rossi et al., 2018) and have now been established for a number of different organs (Liu et al., 2004; Sachs et al., 2019), including the bladder (Lee et al., 2018; Mullenders et al., 2019). Recently, organoids have also emerged as model systems to study host-pathogen interactions during infections caused by bacteria (Bartfeld and Clevers, 2015; Co et al., 2019; Williamson et al., 2018), viruses (Qian et al., 2017; Sanden et al., 2018; Zhou et al., 2018), or parasites (Heo et al., 2018; Nikolaev et al., 2020).

Bladder organoids offer several distinct advantages as model systems for UTIs. They recapitulate the stratified and differentiated layers of the uroepithelium, possess a lumen that mimics the bladder lumen, and are easier to manipulate than whole-animal infection models. Importantly, the compact volume of individual organoids can be imaged in its entirety with a high spatiotemporal resolution using time-lapse confocal microscopy. This makes it possible to follow the rapidly changing dynamics of UTIs and to monitor the responses of host cells and bacterial cell to external perturbations, such as a defined course of antibiotic treatment or the addition of innate immune cells(Neal et al., 2018; Sachs et al., 2019). Compared to conventional *ex vivo* tissue explants or *in vitro* infection models(Andersen et al., 2012) (Justice et al., 2004) bladder organoids offer a more realistic reconstitution of bladder physiology that is accessible to a wider range of experimental techniques for studies of UPEC pathogenesis.

Here, we establish a new model system to study the early dynamics of UPEC pathogenesis based on the recently developed mouse bladder organoids (Mullenders et al., 2019). We use a combination of time-lapse laser scanning confocal microscopy and serial block face scanning electron microscopy (SBEM) to monitor the dispersal, growth, death, and morphology of UPEC within the bladder organoid lumen and wall in response to attack by antibiotics and host neutrophils with single-cell, sub-micron resolution. We find that isolated "solitary" bacteria are seeded in deeper layers of the bladder epithelium at the same time as the formation of IBCs in the superficial umbrella cell layer, which suggests a more diverse and important role for the uroepithelium in general and solitary bacteria in particular in persistent infection, than previously assumed.

Results:

Establishment of differentiated mouse bladder organoids

We generated mouse bladder organoids from C57BL/6 wild-type (WT) or mT/mG mice (Muzumdar et al., 2007), which express the red-fluorescent protein tdTomato within cell membranes, following the procedure of Mullenders *et al.*, (Fig. 1A) (Mullenders et al., 2019). Briefly, mouse bladders were isolated *ex vivo* and epithelial cells extracted from the bladder lumen were cultured in basement membrane extract to generate organoids over a period of 2-3 weeks (Fig. 1A). We verified that these organoids recapitulate the different layers of the stratified mouse uroepithelium by comparative immunofluorescence staining of bladder organoids and explanted mouse bladders. Staining with antibodies directed against uroplakin-3a (UP3a) or cytokeratin 8 (CK8) confirmed the presence of superficial umbrella cells in bladder organoids (Fig. 1B) and mouse bladder tissue (Fig. 1C). CK8 expression was higher in umbrella

cells compared to the underlying intermediate and basal cells, as expected (Southgate et al., 1994). The presence of intermediate and basal cell layers in the bladder organoid was confirmed by staining with antibodies directed against cytokeratin 13 (CK13) (Fig 1B, C), p63 (Fig. S1A, C), or cytokeratin 7 (CK7) (Fig. S1B, D). Bladder organoids therefore recapitulate the stratified architecture of the mouse uroepithelium with high levels of uroplakin expression in the umbrella cell layer, which is important for UPEC adherence and invasion mediated by type I pili(Mulvey et al., 1998).

Invasion of UPEC into the bladder wall provides protection against antibiotics

Intravital imaging of antibiotic treatment and recovery in the infected bladder is extremely challenging(Justice et al., 2004, 2006). We therefore modelled the acute phase of a UTI by microinjecting UPEC expressing yellow fluorescent protein (YFP) into the lumen of individual bladder organoids, which mimics the natural route of infection through the urethra (Fig. 2A). The infection cycle was modelled in three stages: stage one (0-165 minutes), an initial period of unimpeded bacterial proliferation; stage two (165-345 minutes), treatment with ampicillin at ten-fold the minimum inhibitory concentration (10X-MIC); stage three (345-525 minutes), bacterial recovery after ampicillin washout. Snapshots from time-lapse imaging of two organoids are shown in Fig. 2B-E (see supplementary movie SMov1) and Fig. 2F-I (see supplementary movie SMov2); an additional example is shown in Fig. S2A (see supplementary movie SMov3). Rapid bacterial growth within the organoid is observed soon after microinjection (Fig. 2B, C and 2F, G), predominantly within the lumen (indicated by a yellow arrowhead in Fig. 2B). As in UTI infections in humans and in animal models of UTI, bacterial growth over time leads to a gradual exfoliation of umbrella cells, as indicated by reduced CK8 levels (cf. Fig. S3C and controls in

Fig. S3A), while the overall structure of the organoid is relatively unaffected (cf. Fig. S3D and Fig. S3B).

Addition of 10X-MIC ampicillin (64.5 μg/mL, Fig. S2C) into the medium surrounding the organoids rapidly reduces the bacterial volume within the organoid (Fig. 2D, H), consistent with the bactericidal nature of the antibiotic. In most cases, bacterial growth resumed only after the removal of the antibiotic (Fig. 2E). Unexpectedly, in two out of the 124 organoids studied, bacterial growth resumed even in the presence of the antibiotic (Fig. 2I). A time-profile for the growth kinetics of UPEC within the organoids is shown in Fig. 2J and captures these two different behaviors in the presence of antibiotic. A plot of bacterial volume over time within infected organoids during the growth phase confirms that growth is exponential (Fig. 2K) with a median growth rate of 0.017 min^{-1} (Fig. 2M), corresponding to a doubling time of 41.5 min, in agreement with measurements of growth in the mouse bladder(Justice et al., 2004; Scott et al., 2015). During ampicillin treatment, bacterial volume initially increases before plateauing due to filamentation of the bacteria, consistent with the mode of action of Ampicillin (Fig. 2L). Both fluorescence intensity and intra-organoid bacterial volume subsequently decline, with a median killing rate of 0.019 min^{-1} (Fig. S2D). Compared to growth before ampicillin treatment, regrowth after ampicillin washout is significantly slower, with a median growth rate of 0.003 min^{-1}, corresponding to a doubling time of 226.8 min (Fig. 2M).

Interestingly, the spatial distribution of bacterial regrowth after ampicillin washout is very different from the lumenal growth observed after microinjection (cf. Fig. 2E vs 2B, C and Fig. 2I vs 2F, G) and appears to be localized to the bladder wall. These results suggest that, whereas the

lumen or bladder volume may be the preferred site of growth prior to antibiotic exposure, the bladder wall offers a more protective niche for bacterial regrowth after antibiotic treatment. The organoid model allows us to quantify the dynamics of bacterial growth in both these niches (lumen and bladder wall) simultaneously before, during, and after antibiotic treatment.

Neutrophils swarm towards intra-organoid UPEC with three distinct migratory profiles

Organoids are powerful systems to study immune cell responses *in situ* (Nikolaev et al., 2020; Sachs et al., 2019; Yuki et al., 2020), and, in conjunction with long-term live-cell imaging, can be used to visualize the spatiotemporal dynamics of immune cell responses. Peripheral innate immune cells such as neutrophils have been shown to be the first responders in the early phases of bladder infection in the mouse model (Haraoka et al., 1999). We therefore added murine bone marrow-derived neutrophils to the collagen matrix surrounding bladder organoids immediately after microinjection of the organoid lumen with UPEC. Neutrophils were pre-labeled with a CellTracker dye to enable identification. Live-cell imaging revealed three distinct patterns of neutrophil dynamics (see supplementary movie SMov4, SMov5, SMov6). In most cases, neutrophils surrounding an infected organoid migrated towards and accumulated in the lumen, forming aggregates or swarms (Fig. 3A1-3A3, 3B1-3B3). Neutrophil migration into the organoid lumen was consistently accompanied by a reduction in bacterial volume (Fig. 3A2-3A5, Fig. 3B2-3B5, Fig. 3C2-3C5). In some cases, the neutrophil swarms remain within the lumen for >30 minutes (Fig. 3A3-3A5), characteristic of *persistent swarms* (Kienle and Lämmermann, 2016; Lämmermann et al., 2013). In other cases, the swarm rapidly disaggregates after clearance of bacteria within the organoid (Fig. 3B3-3B5), characteristic of *transient swarms*. In a third category, large intra-organoid aggregates of neutrophils do not form; rather, neutrophil numbers

within the organoid fluctuate in response to bacterial numbers. We classified this third category, with fluctuating neutrophil numbers inside the infected organoid, as a *dynamic swarm*. Additional examples for each type of migratory behavior are shown in Fig S5A-C (see supplementary movies SMov7, SMov8, SMov9).

Additional verification of the inward migration of neutrophils is afforded by an examination of the shapes of these cells; neutrophils surrounding the organoid are predominantly spherical in shape, whereas migratory neutrophils adopt elongated shapes (Fig. S6C). Importantly, neutrophils do not migrate towards uninfected 'bystander' organoids, as shown in Fig. 3A, 3B (colored red), which confirms that neutrophils can discriminate between uninfected and infected organoids and directing their movement specifically towards infected organoids.

These neutrophil dynamics are better understood from time profiles of the neutrophil volume within the organoid (amber), the neutrophil volume surrounding the organoid (blue), and the intra-organoid bacterial volume (green), each normalized by the maximum value attained over the time period of the experiment. Data for each parameter are shown in Fig. 3D-F, corresponding to Fig. 3A1-A5, 3B1-B5, and 3C1-C5, respectively; absolutely numbers are shown in Fig. S4 and Fig. S5D-I. Infection of bladder organoids therefore successfully captures the range of neutrophil migratory responses reported from intravital imaging studies, and bacteria within the lumen are effectively cleared by neutrophils independent of the migratory profile adopted.

Bacteria within the wall of the bladder organoid are refractory to clearance by neutrophils

The rapid clearance of lumenal bacteria by migratory neutrophils provides an opportunity to observe niches where bacteria may be protected from neutrophil attacks, such as intracellular bacterial communities (IBCs) (Justice et al., 2004).We observed IBCs in a subset of infected organoids, reinforcing the validity of the organoid model. Fig 4A1-3 shows an example of an IBC that forms and persists despite the presence of a persistent swarm of neutrophils within the organoid that successfully clears the bacteria from the organoid lumen. Live-cell imaging revealed the IBC to be a dynamic, fluctuating structure; for example, in the 15-minute interval between Fig. 4A3 and Fig. 4A4 (see supplementary movie SMov10), the IBC begins to shed bacteria, which are rapidly taken up by nearby neutrophils. A vast majority of the bacteria released from this IBC are processed and killed, as evidenced by loss of YFP fluorescence, within 30 minutes (Fig. 4A5). ; In contrast, Fig. 4B1-5 (see supplementary movie SMov11) shows another example of an IBC that forms in the presence of a persistent neutrophil swarm (white arrowhead, Fig. 4B1-2), but in this case the bacteria shed from this IBC are spread by the neutrophils to different regions of the bladder epithelium (Fig. 4B3-4, cyan arrowheads). Some of these bacteria can persist as isolated bacteria within the organoid wall and resist neutrophil clearance (cyan arrowheads, Fig. 4B5).

Interestingly, we also observed a subpopulation of isolated bacteria within the organoid wall at an early timepoint (yellow arrowheads, Fig. 4B1). The high spatiotemporal resolution allowed us to track three such examples, labelled ‘1’ through ‘3’, over the entire course of the timeseries shown in Fig. 4B1-5 and verify that these bacteria remained refractory to neutrophil-mediated clearance and were located in the bladder wall (Fig. 4B5, yellow arrowheads and corresponding labels). The numbers of these bacteria within the bladder wall that are refractory to clearance was enhanced by the addition of some of the bacteria shed by the IBC (cyan arrowheads in Fig. 4B5).

Even 15 hours after addition of neutrophils, these isolated subpopulations (threshold of detection set at 10 μm^3) persisted within some organoids (Fig. 4C3, 4C4, 3C and analysis in Fig. 3D, 3F, S4C, S5D and S5G), whereas other organoids were successfully sterilized by the neutrophils (Fig. 4C1, 4C2, and analysis in Fig. 3E, S4B and Fig. S5E-I). These two outcomes (persistence and sterilization) occured with roughly equal frequency (Fig. 4D). Live-cell imaging conclusively verified that bacteria shed from IBCs contributed only a portion of these persistent bacteria.

These results demonstrate additional niches within the layers of the bladder epithelium beyond IBCs that can also harbour subpopulations of bacteria that are resistant to clearance by antibiotics or neutrophils. In the latter case, bacterial persistence is independent of the nature of the neutrophil swarm (Fig. 4C3, 4C4). We attempted to localize these persistent bacteria with greater precision, but the spatial resolution of confocal microscopy proved to be insufficient to identify unambiguously the boundaries of the bladder lumen and the precise location of individual bacteria within the organoid wall. We therefore imaged infected organoids using electron microscopy, which provides much higher spatial resolution than optical microscopy.

Volumetric electron microscopy reveals five distinct bacterial niches within an infected organoid

Technical developments in scanning electron microscopy now permit volumetric imaging of large samples using serial block face scanning electron microscopy (SBEM) (Denk and Horstmann, 2004; Hoffman et al., 2020; Maclachlan et al., 2018). High-contrast staining used for the preparation of SBEM samples densely labels cell membranes, which is useful for localizing

bacteria within tissue. We used this imaging method to capture an entire infected organoid at ca. 6 hours after microinjection of UPEC and addition of neutrophils. The organoid was imaged with optical microscopy (Fig. S7A, S7B) prior to staining and resin embedding. It was then mounted inside the scanning electron microscope and serial images of the entire structure collected at a lateral resolution of 30 nm with 100 nm sections separating each image. The imaging parameters allowed us to identify cell membranes, and localize all bacteria in the organoid. In addition, the light microscopy imaging prior to embedding provided a 3D map of the organoid in which we could identify fluoresecently labelled cells such as neutrophils in the final EM image series. We identified a total of 2938 bacteria, classifying them into five distinct subpopulations by way of their locations within in the organoid (Fig. 5A-E, see supplementary movie SMov12).

The majority (62%, n=1821) of bacteria are extracellular and located within the organoid lumen (Fig. 5A). Smaller bacterial fractions are located either as individual solitary bacteria within the cytoplasm of bladder epithelial cells (3.8%, n=111) or within the IBC (13.5%, n=398) (Fig. 5C, D). The small fraction of bacteria located within neutrophils (4.8%, n=141) is probably an underestimate, since bacteria are typically degraded after phagocytic uptake (Fig. 5B). Bacteria within the neutrophils had an altered morphology, likely due to exposure to antimicrobial stresses within the neutrophil. Unexpectedly, we identified a fifth subpopulation of individual "solitary" bacteria, which we term "pericellular" (15.9%, n=467), that is located in between bladder epithelial cells within the organoid wall (Fig. 5E). To the best of our knowledge, this pericellular subpopulation of "solitary" bacteria has not been reported previously, presumably due to the difficulty of whole-bladder imaging with sufficient spatial resolution to identify individual bacteria located between host cell membranes.

A view inside a model of the organoid, created from a 3D map of coordinates of all cells and bacteria, shows the arrangement of the different bacterial classes inside (Fig. 5F). The bacterial population within the irregularly shaped lumen clusters towards the first quadrant (zoom in Fig. 5G), likely indicating the site of injection. Intracellular and pericellular "solitary" bacteria can be found in all areas of the organoid wall (evident in zoom in Fig. 5H). Individual neutrophils can be observed in all areas of the organoid wall as well as the lumen (Fig. 5H), and some of these neutrophils contain numerous bacteria (Fig. S7C). Bacteria within the IBC form a tight cluster below the nucleus of the cell hosting the IBC (Fig. 5F). The protection against phagocytic uptake conferred by intracellular localization is evident from the fact that the IBC remains intact despite the infected cell being surrounded by multiple neutrophils. A plot of the shortest distance of each subpopulation to the organoid lumen is shown in Fig. 5J. It is noteworthy that intracellular and pericellular "solitary" bacteria are found within the deeper layers of the organoid that express intermediate and basal cell markers (Fig. 1C).

We asked whether the intracellular and pericellular "solitary" subpopulations are phenotypically different from bacteria in the organoid lumen. UPEC has been shown to markedly alter flagellar expression and cell shape during bladder infection (Anderson et al., 2004; Lane et al., 2007; Wright et al., 2007). We therefore used immunofluorescence to probe flagellin expression *in situ*. Because paraformaldehyde fixation tends to degrade the signal of bacterial YFP, we used immunostaining against lipopolysaccharide (LPS) and a mask of the organoid shape to label intra-organoid bacteria (cyan) and bacteria surrounding the organoid (green) in Fig. 6A. The corresponding image with anti-flagellin immunostaining (Fig. 6B) shows that a majority of intra-

organoid bacteria have low or no detectable flagellin expression. We applied a threshold on the basis of volume to the intra-organoid bacteria clumps and found that large bacterial clumps (volume greater than 1,000 μm^3) express very low flagellin levels (Fig. 6D), whereas smaller clumps and individual bacteria retain intermediate to high levels of expression (Fig. 6C, Fig. S8B). Thus, bacteria that continue to express flagellin are predominantly singlets or small clusters located within the organoid wall; both observations suggest that these subpopulations correspond to the intracellular or pericellular subpopulations of "solitary" bacteria identified in serial electron micrographs. This point is strengthened by our observation that bacteria within the IBC have severely reduced flagellar expression, (Wright et al., 2007), whereas singlet bacteria surrounding the IBC retain high-level flagellar expression (Fig. 6E).

Scanning electron microscopy (SEM) is a powerful technique to examine surface morphology and overall bacterial shape. We ruptured open an infected organoid using a tungsten needle (Heo et al., 2018) at ca. 6 hours after microinjection with UPEC to gain access to the interior of the organoid (Fig. 6F). We found that the majority of bacteria that were accessible to SEM imaging were located within tight clusters, suggestive of IBC growth (Fig. 6G, H). These bacteria were coccoid in shape and were not flagellated (Fig. 6H), consistent with previous findings (Anderson et al., 2003; Justice et al., 2004). In contrast, a small subpopulation of bacteria from a different spatial location in the organoid was observed that retained flagellar expression (Fig. 6I, J). These observations are consistent with data in Fig. 6C, D. We verified that bacteria from a stationary phase axenic culture retained flagellin expression (Fig. 6K) and were longer than those within IBCs (Fig. 6L). The bladder organoid model is therefore able to recapitulate characteristic morphological features of bacteria within IBCs. It also reveals that the bladder wall also creates

distinct niches including some where the bacteria are rod-shaped and retain flagellin expression. These highlight the effectiveness of organoids as a tool to obtain a wholistic understanding of UPEC pathogenesis.

Discussion

The mouse model is the most common infection model for UTIs but is challenging to study using live-cell imaging. There is also a lack of tractable *in vitro* models that capture the complex 3-D stratified architecture of the bladder and key aspects of the UPEC pathogenesis cycle relevant to clinical disease viz. persistence and recurrence of infection. For example, early efforts by Smith *et al.* (Smith et al., 2006) developed stratified uroepithelial layers from a human cancer cell line on collagen beads through an application of shear stress, but this model does not have a lumen where bacteria can be introduced in a physiological manner. In contrast, Horsley *et al.* (Horsley et al., 2018) developed a model of regions or islands of stratified primary human uroepithelial cells on transwell inserts. In this model, immune cell dynamics are difficult to recapitulate and live-cell imaging is challenging. Lastly, Andersen *et al.* (Andersen et al., 2012) developed a model in which a virus-immortalized human bladder cell line is cultured under flow to mimic micturition. This model, however, does not include a stratified epithelium or the ability to introduce additional cell components. Although other stratified bladder epithelium models have been reported (Cattan et al., 2011; Chabaud et al., 2017; Suzuki et al., 2019), to the best of our knowledge, none of these models has been adapted for infection studies.

Here, we show that bladder organoids fulfill all these requirements. Using bladder organoids embedded in a physiological collagen matrix, we demonstrate: (1) the ability to simultaneously

probe bacterial growth dynamics in a lumen that mimics the bladder volume as well as within the bladder wall, (2) the ability to deliver and remove antibiotics and study the responses of bacteria within these niches to antibiotic treatment, and (3) the ability to study immune cell migration into the organoid in response to infection. Organoids are amenable to long-term live-cell imaging and offer significantly higher throughput than the mouse model as well as the ability to combine cells from transgenic and wild-type mice. These combinations are not possible in simple monolayer systems (Andersen et al., 2012), in more complex stratified systems (Horsley et al., 2018; Smith et al., 2006), or in experiments with extracted bladder tissue (Justice et al., 2004, 2006).

By leveraging these capabilities, we demonstrate that whereas the bladder lumen is likely to be the predominant source of replicating bacteria in a UTI, it is the simultaneous presence of bacteria within the bladder wall that enables these infections to resist clearance by antibiotics or neutrophils. Rapid bacterial growth within the organoid lumen prior to antibiotic treatment contrasts with substantially slower bacterial growth after antibiotic treatment within the organoid wall. Live imaging also revealed the rare occurrence of bacterial growth even in the presence of antibiotic. This phenomenon could reflect either the rare presence of a niche in the organoid where antibiotic penetration is particularly low; alternatively, it could reflect or the emergence of spontaneous resistance, or the fact that bacterial responses to antibiotics are dynamic and heterogeneous, and bacterial growth has been reported even in the presence of bactericidal concentrations of antibiotic (Wakamoto et al., 2013). These dynamic and transient phenotypes are impossible to capture in a mouse model or through conventional measurements of colony forming units. The bladder wall therefore plays a key role in the recurrence of infection by harbouring bacteria in niches where they are refractory to clearance by antibiotics.

We observed similar dynamics for bacterial killing by neutrophils. The spherically symmetric geometry of the organoid model allowed us to capture neutrophil migration dynamics in a quantitative fashion that is difficult to achieve with other systems. We found that UPEC infection of organoids generated a strong and directed neutrophil migration response, with distinctive dynamics that are remarkably similar to reports based on intravital imaging of neutrophil responses to bacterial infections (Lämmermann et al., 2013; Liese et al., 2012; Shannon et al., 2013). We found that neutrophils also migrated out of the lumen of the organoids after resolving infection. Yet across these different migratory profiles, about half of the organoids studied were not completely sterilized by neutrophils even after many hours. This observation reiterates the importance of the niche in the bladder wall that was not restricted to IBCs. Indeed, IBC formation was observed in only a minority of cases.

We further highlight the power of the organoid approach by using SBEM to locate every bacterium within an infected organoid. The greatest fraction of bacteria were within the lumen; while it can be argued that our model exaggerates the occurrence of growth in the lumen due to the lack of clearance by urination, the closed volume of the lumen sets an upper limit on bacterial numbers, which is unlikely to be found in an *in vivo* setting. This dataset revealed some surprising results. IBCs were not the only niche in which bacteria were found within the organoid wall. A substantial fraction of bacteria was present as singlets either within epithelial cells (intracellular) or between epithelial cells (pericellular).

The small volume of the organoid lumen and the lack of clearance by urination might accelerate the formation of IBCs relative to the mouse model. Still, it is noteworthy that IBCs as well as intracellular and pericellular "solitary" subpopulations, although spatially distinct, all form within hours of infection. Studies from the mouse model have established a timeline wherein repeated cycles of IBC growth and fluxing eventually leads to the formation of a "quiescent reservoir" about 2 weeks after infection. Implicit in this scheme is the assumption that IBCs are an intermediate step in the formation of quiescent reservoirs. Here, we provide evidence that subpopulations of "solitary" bacteria can be seeded within deeper layers of the bladder epithelium at much earlier times, coincident with the formation of IBCs. Some of these intracellular or pericellular "solitary" bacteria may eventually develop into quiescent reservoirs; however, we could not test this possibility within the relatively short timescale of our experiments.

The intracellular and pericellular "solitary" bacteria appear to be phenotypically distinct from bacteria within an IBC, inasmuch as they remain rod-shaped and flagellated, whereas bacteria within an IBC are coccoid-shaped and unflagellated. The latter point is interesting because flagellar expression is important for generating persistent infection in the bladder(Lane et al., 2007; Wright et al., 2007) yet the loss of flagellar expression within IBCs has been reported in numerous studies (Wright et al., 2007). Our data suggest that unflagellated bacteria within IBCs and flagellated "solitary" bacteria seeded throughout deeper layers of the bladder wall may both contribute to persistence. Given the relatively small numbers of "solitary" bacteria, it is unlikely that this subpopulation could be identified by transcriptomic analysis of the total bacterial population within the bladder.

The dynamics of host-pathogen interactions during bladder infections are difficult to capture in bulk experiments in conventional animal models. Bladder organoids, being miniaturized and experimentally tractable models of the bladder, are excellently placed to reveal new insights into UPEC pathogenesis. Here, we leverage these features to demonstrate the existence of “solitary” subpopulations of intracellular and extracellular bacteria located within deeper layers of the bladder organoid wall. These “solitary” subpopulations appear early in the course of infection, concomitant with the formation of IBCs, and they resist elimination by antibiotics and neutrophils. Thus, improved understanding of the physiology of “solitary” bacteria could contribute to the development of new strategies to eliminate persistent bladder infections.

Figures:

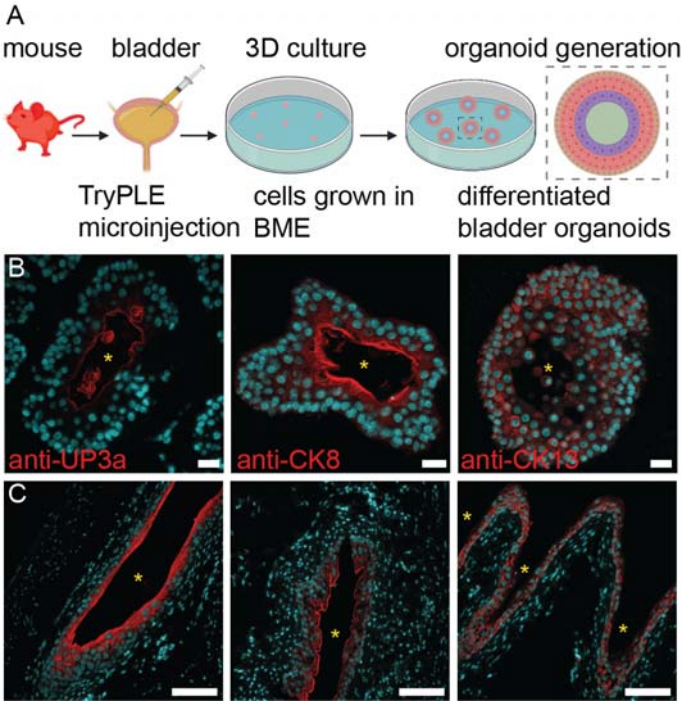

Figure 1: Mouse bladder organoids recapitulate the stratification of bladder uroepithelium.

(A) Schematic of the protocol used for generation of mouse bladder organoids. Lumenal cells, isolated by microinjection of TryPLE solution into the bladder, are cultured in basement membrane extract (BME) to form differentiated bladder organoids. (**B, C**) Immunofluorescence staining confirms that bladder organoids (**B**) recapitulate the stratified layers of the uroepithelium observed in mouse bladder tissue (**C**). The umbrella cell layer was identified with anti-uroplakin3a (anti-UP3a) and anti-cytokeratin8 (anti-CK8) antibodies. The basal and intermediate cell layers were identified with anti-cytokeratin13 (anti-CK13) antibody. Cell nuclei were labeled with DAPI (cyan). The lumens of the bladder organoids and mouse bladder slices are indicated by yellow asterisks. Scale bars, 20 μm in (**B**) and 100 μm in (**C**).

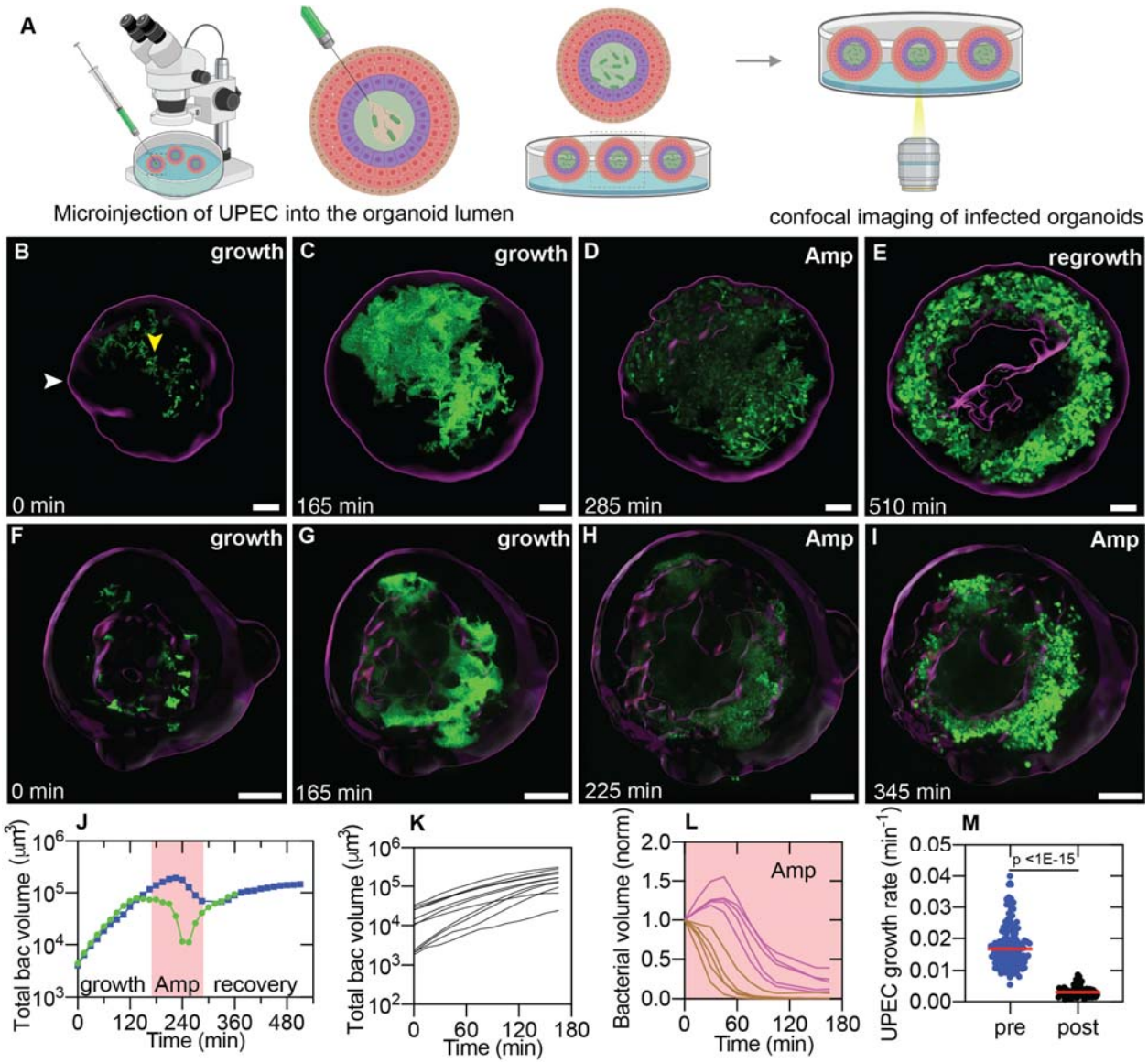

Figure 2. Bacteria within the bladder organoid wall are refractory to antibiotic clearance. (**A**) Schematic of the microinjection protocol. Bacteria are injected via a glass microcapillary into the lumen of individual organoids and the organoids are resuspended in a collagen matrix for live imaging. (**B-E**) Snapshots from time-lapse imaging of an infected organoid over 9 hours acquired by confocal microscopy. (**B**) White arrowhead refers to the organoid boundary. Yellow arrowhead indicates bacteria in the lumen. Bacterial volume within the organoid increases rapidly during the initial growth phase (**B, C**, 0-165 min from the start of the experiment) and

occurs predominantly within the lumen. At ca. 165 min, a 10X-MIC dose of ampicillin was added to the extracellular growth media. (**D**) Intra-organoid bacterial volume, quantified by bacterial fluorescence, decreases due to bacterial killing during this period (ca. 165-345 min). Subsequently, the antibiotic was withdrawn (recovery phase ca. 345-525 min) and bacterial regrowth appears to be restricted to the organoid wall (**E,** see supplementary movie SMov1). In contrast, panels (**F-I**) highlight an isolated example where bacterial volume initially decreases (compare **H** vs **G**) but growth subsequently resumes (**I**) even in the presence of the antibiotic, (see supplementary movie SMov2). (**J)** Time profiles for intra-organoid bacterial volume over the entire course of the experiment for the organoids in panels **B-E** (squares) and **F-I** (circles), respectively. Shaded region represents the period of antibiotic treatment. (**K-M**) Characterization of bacterial growth dynamics at different stages of the experiment. (**K, L**) Representative plots of bacterial volume vs. time reveal that growth is exponential during the pre-ampicillin phase (**K**, n = 11 organoids) and decay is exponential during ampicillin treatment (**L**, n = 10 organoids). In some cases, bacterial volume declines immediately after ampicillin administration (**L**, brown lines), while in others, growth continues for some time before declining (**L**, magenta lines). (**M**) Scatter plot for the growth rate of the bacterial volume within the bladder organoids before and after ampicillin exposure (n=124 and n=58 organoids, respectively). Growth rates before and after ampicillin treatment are significantly different ($p<1E-15$, calculated using a Mann-Whitney Test). Red lines represent the median values. Scale bars, 20 μm in (**B-I**).

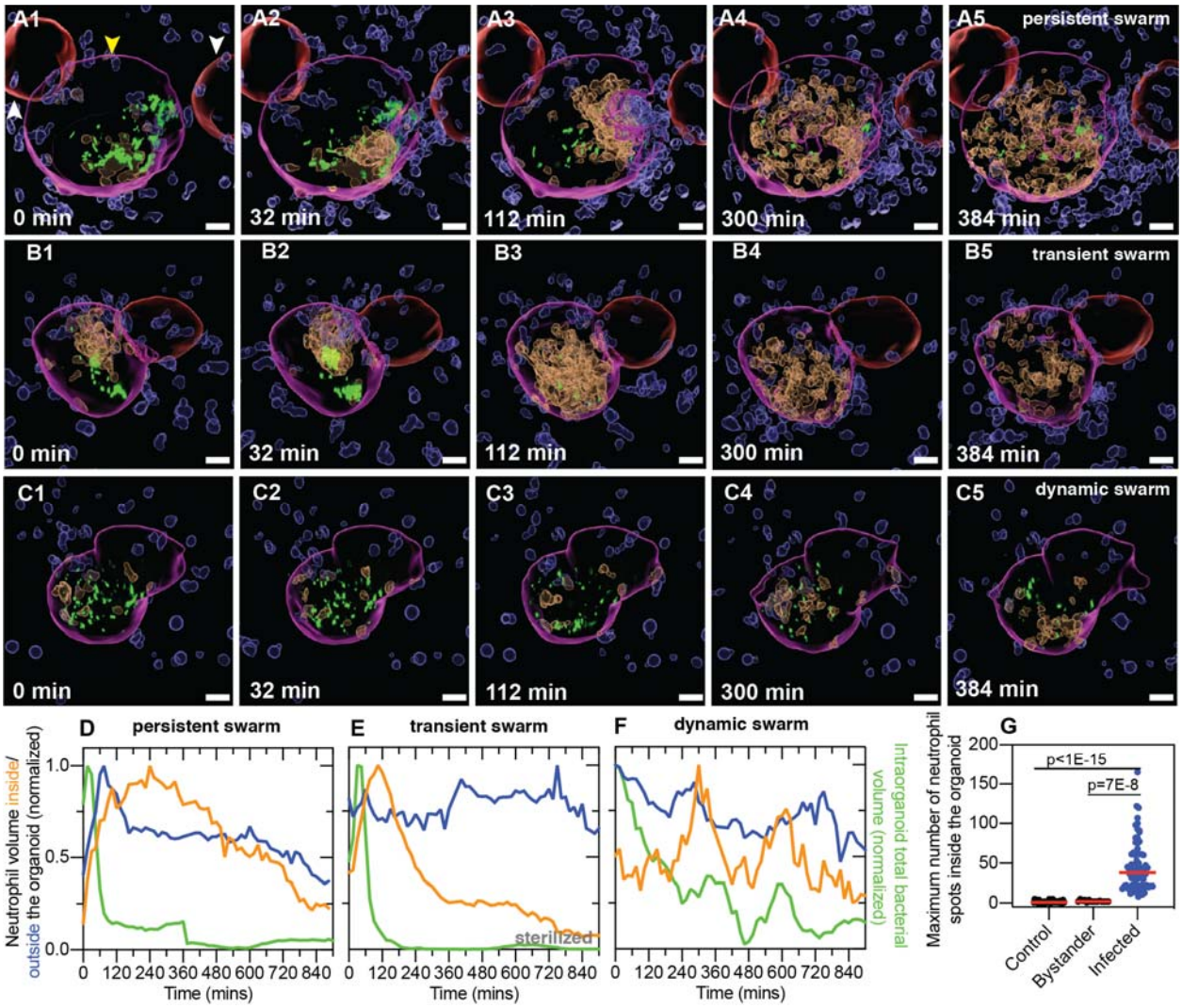

Figure 3. Neutrophil swarming dynamics in response to bacterial infection.

Characterization of neutrophil migration dynamics by time-lapse imaging of infected mouse bladder organoids. In all panels, surfaces of intra-organoid (amber) and extra-organoid (blue) neutrophils and infected (magenta) and uninfected (red) organoids were generated using a Bitplane Imaris analysis pipeline. UPEC (green) are shown without processing to identify individual bacteria. (**A1-A5**) **Persistent swarm.** Snapshots show the migration of neutrophils into the lumen of an infected organoid (yellow arrowhead) but not the adjacent uninfected organoid (white arrowhead). A neutrophil swarm forms around the bacteria in the lumen and persists over the course of the experiment. Individual "solitary" bacteria in the bladder wall (**A5**)

appear to be refractory to clearance. Images are presented in a perspective view. (**B1-B5**) **Transient swarm.** The image series shows two consecutive cycles of swarm formation and disaggregation in response to intra-organoid bacterial growth. (**C1-C5**) **Dynamic swarm.** The image series shows rapidly fluctuating neutrophil numbers within the organoid without the formation of large aggregates. (**D-F**) Time profiles of the relative volumes of neutrophils within the organoid, neutrophils surrounding the organoid, and bacteria within the organoid for the three profiles presented in (**A-C**), respectively. In each case, the volume is normalized to the maximum volume during the course of the experiment. Persistent and transient swarms are characterized on the basis of neutrophil reverse migration rates. (**G**) Scatter plots of the maximum number of intra-organoid neutrophils during the experiment in uninfected control organoids, uninfected bystander organoids, and infected organoids provides clear evidence of directed migration into infected organoids. $P<1E-15$ comparing control organoids ($n = 30$) and infected organoids ($n = 75$). $P=7E-8$ comparing bystander organoids ($n = 15$) and infected organoids ($n = 75$). P-values were calculated using Kruskal-Wallis ANOVA Test. Red lines represent median values. Scale bars, 20 μm in (**A1-C5**).

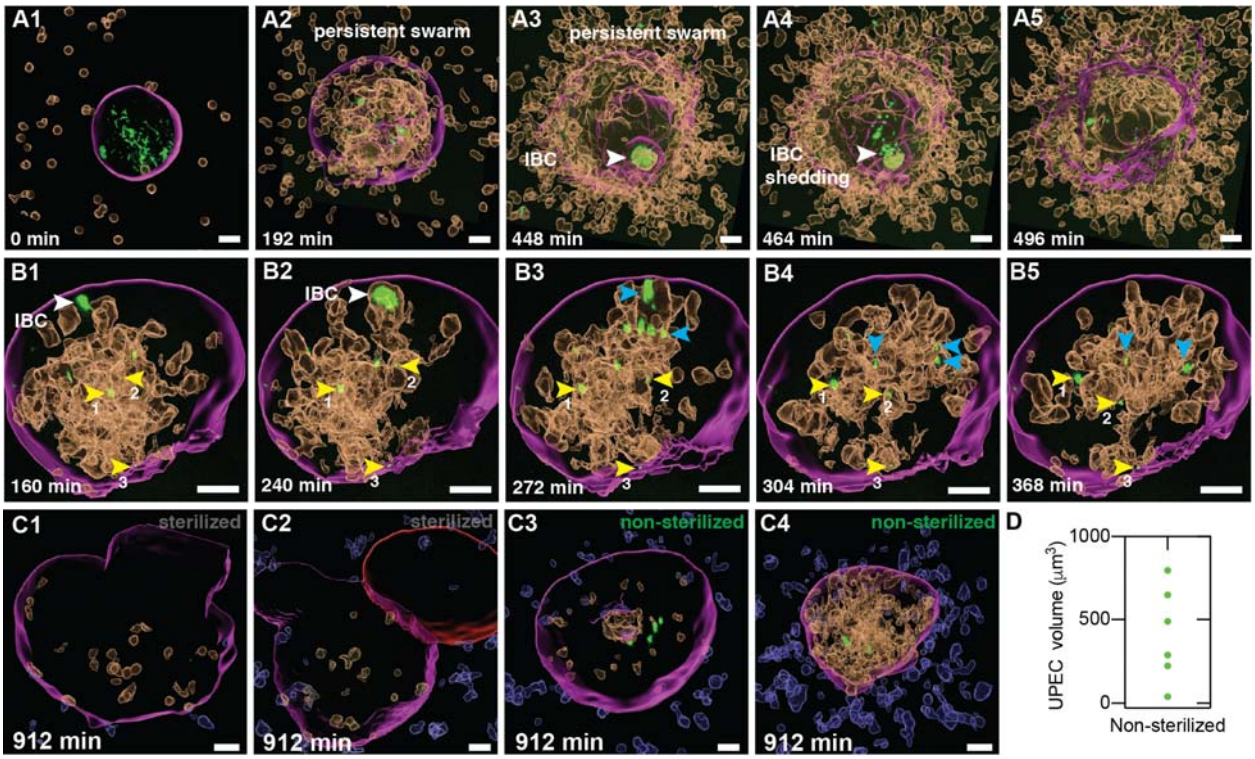

Figure 4. Bacteria within the bladder organoid wall are protected from clearance by neutrophil swarms.

(**A1-A5**, **B1-B5**) Two examples of IBCs that are protected from neutrophil-mediated clearance. Shedding of bacteria from an IBC (**A4, A5** and **B2, B3**) is followed by two outcomes: phagocytic uptake and rapid clearance (**A5**), or dispersal to other niches in the bladder epithelium (**B5**, cyan arrowheads). Three examples of isolated solitary bacteria in the bladder wall (labelled '1', '2' ad '3') that are refractory to clearance throughout the timeseries in (**B1-B5**) are indicated by yellow arrowheads and tracked within the organoid over this time period. (**C1-C4**) Snapshots at ca. 15 hours after infection and addition of neutrophils. (**C1**, **C2**) Examples of organoids, where UPEC are cleared, following neutrophil treatment. (**C3**, **C4**) Examples of bacterial persistence in organoids where the neutrophil swarm disperses (**C3**) or persists up to 15 hours post-infection

(**C4**). (**D**) Quantification of the total bacterial volume at 15 hours post-infection in case of non-sterilized organoids (n=6). Scale bars, 20 μm in (**A1-A5**), (**B1-B5**), and (**C1-C4**).

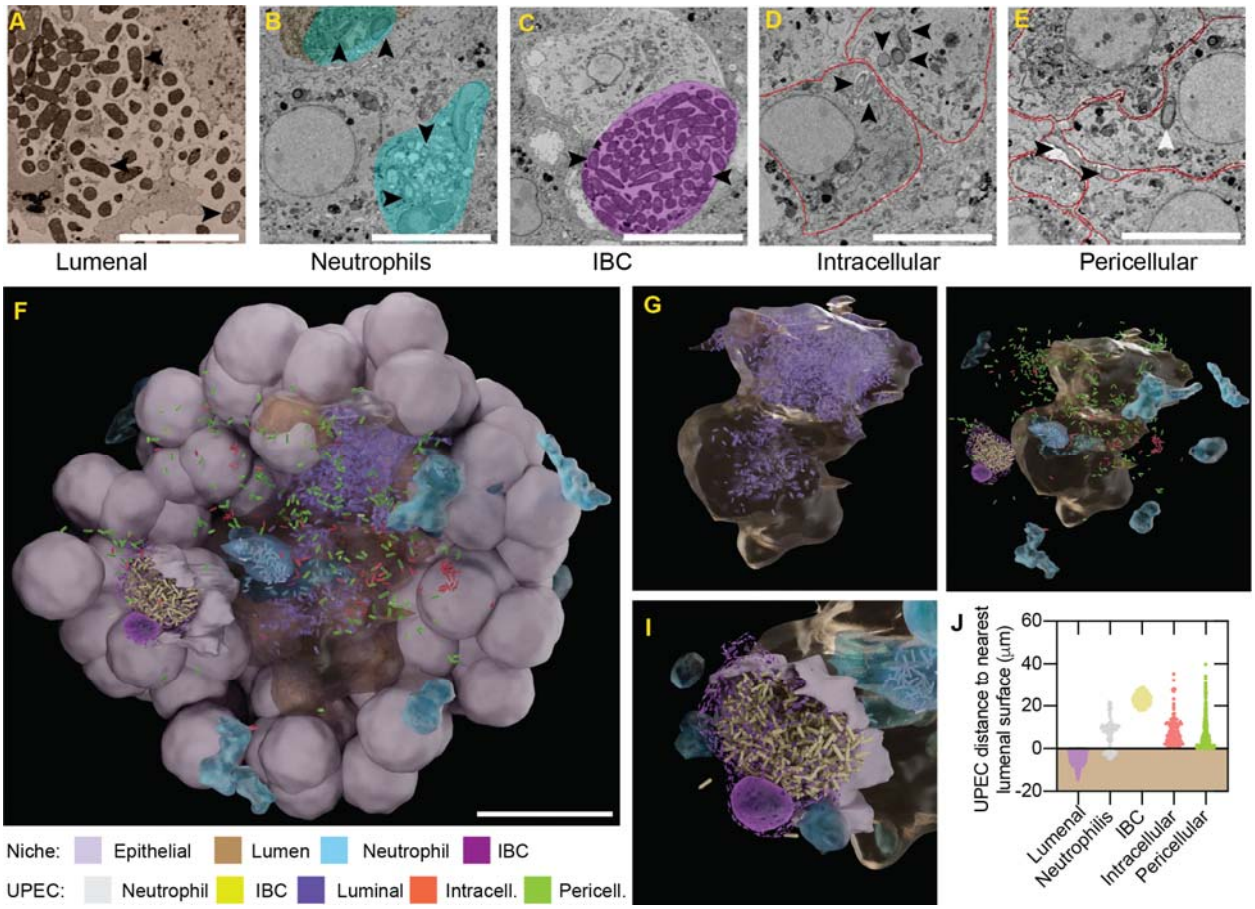

Figure 5: Volumetric electron microscopy reveals five distinct bacterial niches within an infected organoid.

(**A-E**) Serial-block face-scanning electron microscopy (SBEM) snapshots of an infected organoid at ca. 6 hours after microinjection of UPEC and addition of neutrophils. Five distinct niches were clearly identified and the bacteria in each niche (**A-E**) are indicated by black arrowheads. (**A**) Extracellular bacteria within the organoid lumen (brown; n = 1,821). (**B**) Bacteria within neutrophils (light cyan) that can be either in the lumen or in the bladder epithelium (n = 141). (**C**) Bacteria within an IBC (yellow; n = 398). The cytoplasm of the IBC is shown in purple. (**D**) Individual bacteria in the cytoplasm of epithelial cells (cell boundaries in red; n = 111). (**E**) Bacteria located between epithelial cells (cell boundaries in red; n = 467). An additional example of an intracellular bacterium is indicated with a white arrowhead. (**F**) Model

derived from the serial electron microscopy images of the entire organoid in which all bacteria and cells were plotted. Image shows the interior of the organoid, revealing the lumen (brown), and epithelial cells (grey), as well as the neutrophils (cyan). Bacteria located within the five niches corresponding to (**A**-**E**) are colored violet (lumenal), grey (neutrophil), lemon yellow (IBC), red (intracellular), and green (pericellular). The width of this organoid is 85 µm. (**G**) Zoom shows the extracellular bacteria in the lumen (brown). (**H**) Zoom shows all other bacterial classifications around the lumen. (**I**) Zoom shows the bacteria within the IBC, which appear to be protected from clearance by the surrounding neutrophils. (**J**) Scatter plot of the distance of bacteria within each subpopulation from the lumenal surface; lumenal bacteria are located entirely within the lumen (shaded brown region). Scale bars, 5 µm in (**A-E)** and 20 µm in **F**.

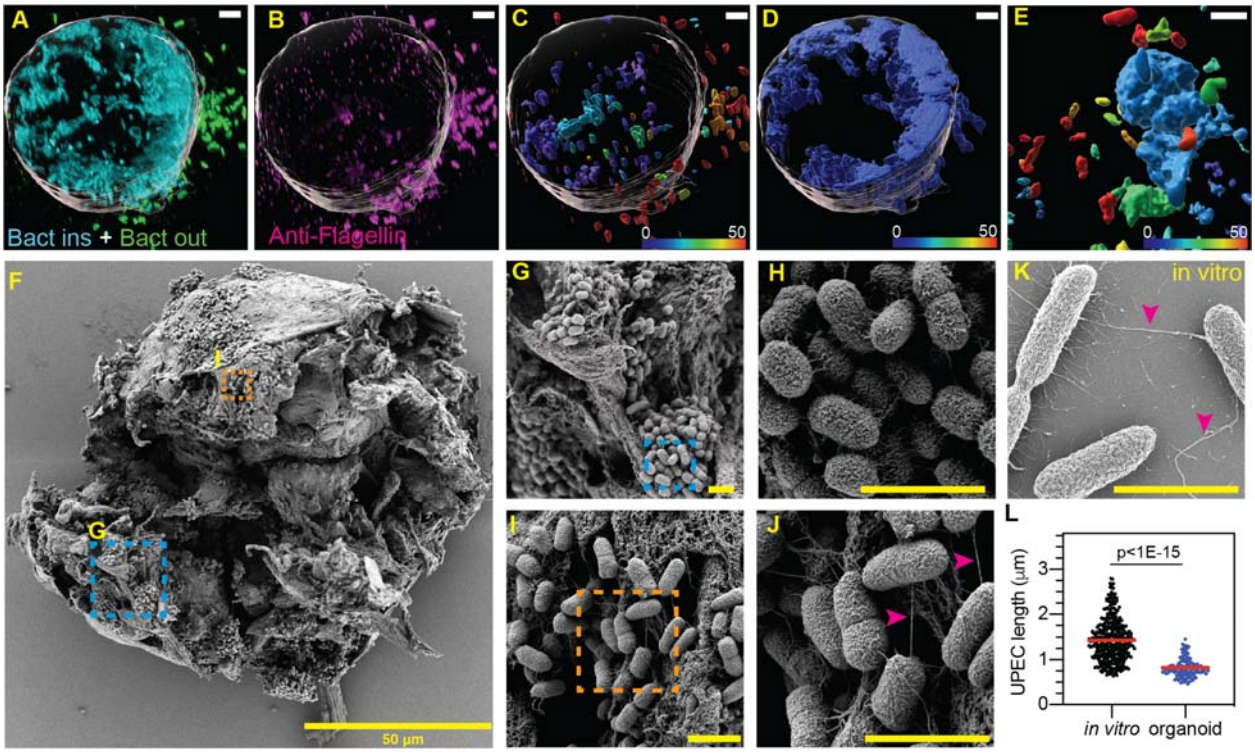

Figure 6: Individual bacterial cells within the bladder organoid wall retain flagellar expression, whereas coccoid forms are non-flagellated.

(**A-D**) Perspective views of an infected organoid (surface indicated in grey) at ca. 6 hours after microinjection with UPEC. (**A**) Bacteria inside (cyan) and outside (green) the organoid were identified by immunostaining for bacterial LPS. (**B**) Flagellated bacteria (magenta) were identified by immunostaining for bacterial flagellin. Analysis of co-expression of LPS and flagellin for individual bacteria (**C**) or large clumps of bacteria, which are predominantly restricted to the lumen (**D**). Bacteria are color-coded according the intensity of the flagellin signal. Flagellated bacteria are predominantly observed outside the organoid (**C**) but can also occur as individual "solitary" cells within the organoid wall. (**E**) Bacteria within an IBC have low-level flagellin expression, whereas individual bacteria surrounding the IBC retain high-level flagellin expression. (**F**) Scanning Electron Microscopy (SEM) image of an infected organoid at 6 hours after microinjection with UPEC. Ruptured organoids reveal multiple areas of bacterial

growth. Zooms for two representative areas are shown in (**G-J**). Bacteria in (**I**) are loosely packed, rod-shaped, and express flagella (**J**, magenta arrowheads), whereas bacteria in (**G**) are tightly packed, coccoid-shaped, and do not express flagella (**H**). (**K**) SEM image of UPEC grown in axenic culture, where flagellar expression in rod-shaped bacteria is clearly observed (magenta arrowheads). (**L**) Size distributions for bacteria grown to stationary phase in axenic culture and bacteria within tightly-packed clusters in the organoid. Both populations were imaged by scanning electron microscopy. Bacteria in axenic cultures (n=370) are longer than intra-organoid bacteria (n=136) ($p<1E-15$, calculated using Mann-Whitney Test). Scale bars, 5 μm in (**A-E)** and 2 μm in (**F-K)**.

Materials and Methods

Generation of mouse bladder organoids from mouse bladder uroepithelial cells

Mouse bladder organoids were prepared by selectively isolating lumenal cells from the bladder of C57BL/6 (Charles River Laboratories) or ROSA$^{MT/MG}$ (Jackson Laboratories) by filling the clamped mouse bladder *ex vivo* with TrypLEA as described in a recent study (Mullenders et al., 2019)). Mice were housed in a specific pathogen-free facility. Animal protocols were reviewed and approved by EPFL's Chief Veterinarian, by the Service de la Consommation et des Affaires Vétérinaires of the Canton of Vaud, and by the Swiss Office Vétérinaire Fédéral.

Briefly, mice were euthanized using CO_2 overdose and lumenal uroepithelial cells were isolated from 3 female mice at an age of four months to optimise the number of uropeithlial cells obtained by microinjecting approximately 500 µL TryPLE (Gibco) with a 26G needle (Terumo) and placing the clamped mouse urinary bladder inside a 50 mL Falcon tube surrounded by pre-warmed 20 mL basal medium (Advanced DMEM/F-12 medium). The Falcon tube containing mouse urinary bladder is incubated for 1 hour inside a cell culture incubator at 37°C and 5% CO_2. The mouse urinary bladder is then washed twice with basal medium containing 20% heat-inactivated fetal bovine serum (FBS) to neutralize the effect of TryPLE. The cell suspension was passed through a 40 µm filter (Fisher) and the flow-through cells were collected, centrifuged and pelleted at 0.3 g for 5 minutes. The isolated uroepithelial cells were resuspended in an appropriate volume of Cultrex® Basement Membrane Extract (BME) and seeded as hemispherical domes (with 40-50 µL volume) in 24-well plate. The 24-well plate is inverted to promote 3D growth and BME is allowed to polymerize at 37°C for 30 minutes. The solidified hemispherical domes are supplemented with mouse bladder medium (MBM, (Mullenders et al.,

2019)) supplemented with 1X antibacterial/antifungal solution (Gibco). MBM medium consists of [Advanced DMEM/F-12 (Thermofischer), 100 ng/mL of FGF10 (Peprotech), 25 ng/mL of FGF7 (Peprotech), 500 nM of A83-01 (Tocris Bioscience), 2% of B27 (Thermofischer) and ROCK inhibitor (Y-27632, 10 μM)]. Over the subsequent 2-3 weeks, the uroepithelial cells mouse bladder organoids MBOs were passaged in 5 days or sheared with a fire polished glass pipette. MBOs were either used immediately for infection experiments or cryopreserved in the freezing media (60% FBS, 30% Advanced DMEM/F-12 and 10% DMSO) at -180°C for later experiments.

UPEC culture and Injection of mouse bladder organoids

Uropathogenic Escherichia coli (UPEC) strain CFT073 isolated from a pyelonephritis patient used for all experiments was a kind donation from Harry L. T. Mobley. A strain expressing yellow fluorescent protein (YFP) episomally was generated by electroporation with the PZA32-YFP plasmid. To induce the expression of type 1 pili, UPEC was grown in LB media containing 25 μg/mL chloramphenicol in non-shaking condition at 37°C for 2 days prior to the experiment.

Cryopreserved tdTomato MBOs were thawed, and recultured in BME for five days before the experiment. One day before the experiment, tdTomato MBOs were washed twice with ice cold DMEM (without antibacterial/antifungal) followed by centrifugation at 0.1 g for 5 minutes to remove old BME. They were then seeded in fresh BME inside a 35 mm ibidi μ-Dish in basal medium without antibacterial/antifungal supplementation. On the day of the experiment, stationary phase UPEC were microinjected into the lumen of MBOs using a Pneumatic

PicoPump (WPI). The micropipettes used for microinjection were prepared by laser pulling of thin wall glass capillary (TW100F-4 with length=100 mm, diameter= 1mm) with Flaming/Brown Micropipette Puller (Sutter Instruments model P-87) with following conditions (Pressure=360, Heat=866, Vel=200). Prior to UPEC microinjection, micropipettes were filled with 10 µL of 1:1 volume dilution of UPEC culture with a Phenol Red solution (Sigma-Aldrich:) using Microloader™ flexible tips (Eppendorf). This allowed the injected volume to be observed. The micropipettes were broken with a sharp scalpel under a stereomicroscope (Olympus SZX-16). The tip size of the cut micropipette was checked by setting pressure conditions on PicoPump to eject 1nL volume in mineral oil on thin film of paraffin on a Zeiss coverslide (corresponding to 100 µm). 1nL of diluted bacterial volume corresponds to 100-200 UPEC bacilli (assessed by plating for colony forming units (cfu) on LB plates). The volume of bacterial inoculum was adjusted according to the size of tdTomato MBOs. Medium sized organoids (100-300 µm in diameter) with a clearly distinguishable lumen were the easiest organoids to inject.

For the experiments with co-culture with mice neutrophils, injected organoids were removed from fresh BME by pipetting 2 mL of ice-cold Cell Recovery Solution (Corning™) after removing MBM from ibidi µ-Dish. The BME hydrogel was mechanically dissociated with a P1000 pipette and resulting liquid gel was placed inside a 15mL falcon tube pre-coated with a 1% BSA solution. The ibidi µ-Dish was washed with additional 1.5 mL of Cell Recovery Solution twice to collect the organoids and, the resulting 5 mL of Cell Recovery Solution containing MBOs inside the 15 mL falcon tube was occasionally mechanically dissociated with non-tapered glass pipette pre-coated with a 1% BSA solution The cell recovery solution containing infected organoids was kept on ice for 30 minutes to completely liquify the BME. The

cell recovery solution was then exchanged through two washes with 10 mL of basal medium (supplemented with 10% FBS) and the organoids were centrifuged at 0.1 g for 5 minutes at 4°C to remove the recovery solution. The organoid pellet was then ready to be resuspended in a collagen gel.

Isolation of neutrophils and labelling with cell tracker

3 female WT mice (Charles River) were used per experiment to isolate neutrophils from bone marrow. Mice were euthanized using CO_2 overdose, and the femur and tibia were isolated. The isolated bone marrow was crushed with a mortar and pestle and subsequently resuspended in 5 mL of cold SM++ solution (HBSS + 2% serum + 25 mM HEPES). The tissue homogenate was then passed through a pre-wet 40 μm filter. Additional cold SM++ solution was added to the filtered cell suspension to make a total volume of 50 mL and then pelleted down at 0.3 g for 5 minutes. The cell suspension was then processed in batches of 10^7 cells using positive selection with the Miltenyi Anti-Ly6G kit as described by the supplier. Isolated Ly6G mice neutrophils were stained with CellTracker™ Deep Red (Thermofisher) in a serum free RPMI phenol red free medium at 1μM concentration and incubated for 30 minutes in 5 mL cell suspension inside 50 mL falcon tube maintained at 37 □. Post-CellTracker™ labelling, labelled mice neutrophils were washed twice with 10 mL of 20% FBS in RPMI phenol red free medium to remove the unbound dye. The labelled neutrophils were kept briefly on room temperature till introduced into a co-culture with infected organoids inside the collagen gel.

Co-culture of mice neutrophils and infected organoids in collagen gels

Collagen gels were used to o-culture infected organoids and mice neutrophils. The collagen gel master mix buffered at pH 7.0 is made by adding 312 µL of ice-cold native Bovine collagen with 4 µL of 1M HEPES, 4 µL of 1M sodium bicarbonate, 40 µL of 1X DMEM/F-12 and 40 µL of 10X DMEM/F-12. The collagen gel mixture is temperature-sensitive and so must be maintained on ice. Care should also be taken to avoid generating bubbles when pipetting. 10^7 Freshly isolated and CellTracker^{TM} labelled neutrophils were first resuspended in 88 µL volume of premade mixture of collagen gel master mix (10X DMEM/F-12, 1X DMEM/F-12, HEPES, sodium bicarbonate) without native bovine collagen on ice. The resuspended neutrophils wee then mixed with infected organoids. 156 µL of collagen solution was added twice to resuspended neutrophils-organoids mix on ice followed by rapid mixing with a P200 pipette. The obtained collagen gel mix of infected organoids-neutrophils was pipetted on a pre-plasma treated ibidi µ-Dish (pressure =60, time =60 s, Diener). The plasma treatment makes the µ-Dish surface more hydrophilic and allows for a uniform thin layer (1-2 mm) of collagen gel to be deposited on the dish which is good for imaging with a confocal microscope. The collagen gel was then incubated at 37°C and 5% CO_2 for 30 minutes to allow the collagen gel to polymerize and solidify. Lastly, 1.5 mL (supplemented with 25 ng/mL of murine Granulocyte – Colony Stimulating Factor (G-CSF) was supplemented to the co-culture of infected organoids and neutrophils.

Immunofluorescence of uninfected / infected mouse bladder organoids

Cryopreserved MBOs were thawed and maintained in BME culture five days before the experiment. The cultured uninfected/infected MBOs were fixed with 4% paraformaldehyde (PFA)for 6 hours at RT with occasional mechanical dissociation with a P1000 pipette. The fixed

organoids were then washed with PBS and then centrifuged at 800 rpm for 5 minutes in a 1% BSA pre-coated 15mL falcon tube. The organoids were washed at least twice with PBS to remove any remaining residues of PFA. The organoids were then resuspended in 50 µL of prewarmed Histogel at 50 ^{o}C and pipetted out as a small hemispherical dome inside a 1 cm Tissue-Tek Cryomold. The cryomold was placed on a cold ice plate for solidification. Subsequently, the hemispherical Histogel was processed either for paraffin embedding or cryofixation. Organoids embedded in paraffin/cryosections are cut into 4 µm slices. The thin paraffin sections were deparaffinized and rehydrated by immersing the slides through following solutions (Xylene : three washes for 5 minutes each, 100% Ethanol : two washes for 10 minutes each, 95% Ethanol : two washes for 10 minutes each, 70% Ethanol : two washes for 10 minutes each, 50% Ethanol : two washes for 10 minutes each and PBS : washes for 5 minutes each). Rehydrated slides were then processed for heat induced antigen retrieval using 10 mM citrate buffer pH = 6. Slides were washed with 1X PBS, permeabilized with 0.15 % Triton X-100 for 15 minutes, washed twice with 1X PBS, blocked with 1% BSA in PBS for 1 hour. The boundaries of paraffin sections were marked with a hydrophobic pen and slides were labelled with permanent ethanol resistant marker. Primary antibody incubation at a dilution of either 10 µg/mL or 1:100 was performed overnight in a solution of 1% BSA, 0.01% Triton-100 in PBS (antibody incubation buffer). The slides were subsequently washed three times with PBS for 10 minutes each. Secondary antibody incubation was performed at 2 µg/mL in antibody incubation buffer for 1 hour at RT. Excess antibody was removed by washing three times with PBS for 10 minutes each. Cell nuclei were stained with DAPI (5 µg/mL) for 30 minutes and Slides were mounted with Fluoromount-G^{TM} mounting medium (Thermofisher) overnight in a dark chamber.

For the immunofluorescence of MBOs cultured for 6 hours in collagen gels on Ibidi µ-Dish, uninfected/infected MBOs were fixed with 1 ml of 4% PFA for 1 hour. Antibody labelling was performed as described above. The images were deconvolved using SVI Huygens (Quality- 0.05, Iterations=40).

Time-lapse imaging of infected organoids using confocal microscopy

All imaging experiments were conducted using a Leica SP8 confocal microscope in the inverted configuration with a temperature controlled microscope environmental chamber at 37°C and a stage-top chamber that allowed supplementation with 5% CO_2 (OKOlabs). Time-lapse imaging was conducted using a Leica HC FLUOTAR 25X (NA=0.95) multi-immersion objective. Water was pumped to the ring around the water objective with software (SRS signal, 9 Hz, pumping duration - 10 seconds, pumping interval - 30minutes). Microinjected tdTomato MBOs were identified and imaged with 2 or 3 channels for infected organoid incubated without or with neutrophils respectively. The laser excitation wavelengths: 500nm (YFP), 555 nm (td Tomato) and 630 nm (CellTracker^{TM} Deep Red) were chosen to allow multi-channel imaging within the same sequence with reduced spectral overlap. Images were acquired with a scan speed of 700 Hz and a zoom factor of 2.25 that resulted in an XY resolution of 200 - 450 nm depending on the number of pixels acquired per field of view. Z-stacks were acquired with 0.5 or 1 µm step sizes.

Experimental setup and image analysis for ampicillin experiments

As described, freshly BME suspended tdTomato MBOs were microinjected with UPEC. Post UPEC microinjection, MBOs were resuspended in collagen and supplemented with 1.5 mL of MBM medium post collagen polymerization for 30 minutes. Prior to the experiment, the ibidi µ-

Dish were modified by inserting bent metallic tubes (1.00/0.75 X 20mm, Unimed Catalogue 200.010-A) through the lid and sealing these devices with PDMS cured in an oven at 80 ^{o}C for 1 hour. Flexible tubing (0.76x1.65x1, Mono-Lumen Freudenberg medical) connected to these tubes allowed for medium addition and removal. A period of 2 to 3 hours was typically required to set up the experiment on the microscope and is not considered within the time duration of this experiment. Once imaging commenced, bacteria were allowed to grow for 3 hours (0-165 minutes, referred to as growth phase. The media in the mu dish was then replaced with fresh media containing Ampicillin (64.5 µg/mL, 10X MIC). The dynamics of bacterial growth in the presence of ampicillin was monitored for the subsequent 3 hours (ca. 165-345 minutes, referred to as the Ampicillin phase). The Ampicillin was removed from the extracellular medium by slow exchange with fresh MBM media with a 10 mL syringe. The bacterial regrowth was then monitored for a further 3 hours (345-525 minutes, referred to as regrowth phase). The drift in focus was adjusted manually at frequent intervals throughout this experiment.

Image analysis for confocal live imaging

Image analysis was performed with Bitplane Imaris 9.5.1. The time lapse images have four channels (UPEC-first channel, epithelial-second channel, neutrophils-third channel, transmitted light-fourth channel). Organoid surface was generated and tracked over time using the second channel with parameters (Threshold 5 to 15), Smooth (Surfaces Detail-3 µm)). When required, nearby organoids were separated with seed point diameter (depending upon the size of nearby organoids) or adjoining organoid surfaces orthogonally trimmed with the cut option. The epithelial channel was subtracted from the neutrophil channel to create a fifth channel

(neutrophils-epithelial). This channel subtraction was performed to reduce the cross-talk between the boundaries of the epithelial cells marked by the tdTomato membrane marker and neutrophils labelled cytoplasmically with CellTracker Deep Red. This allowed for a more robust detection of neutrophils inside the organoids. Finally, the organoid surface was used to mask the fifth channel and generate a sixth channel of intra-organoid neutrophils. This masked sixth channel was used to detect neutrophil surfaces (Threshold-10, surface smoothness-0.5 or 1) and neutrophil spots (8 µm in size, Quality- 4 to 8) inside the organoid. Neutrophil spots in the field of view were detected with neutrophil channel with parameters (8 µm in size, Quality- 4 to 8). Neutrophil surfaces in the field of view were detected with third channel. Neither neutrophil spots nor neutrophil surfaces were time tracked due to the technical difficulties with imaging speed and amorphous shapes of migrating neutrophils around infected organoids. Average neutrophil sphericity (>=0.5) for neutrophils around an organoid was obtained with time-collapsed information of average neutrophil sphericity for all the neutrophil surfaces per time point. In cases of bigger neutrophil clusters, average neutrophil sphericity was obtained by excluding sphericity of the bigger neutrophil cluster (<0.5). For UPEC volume inside the organoids, first channel was sufficient to create the surface (Threshold-15, Smooth (Surfaces Detail-0.5 or 1 µm)). In cases of extracellular UPEC growth, organoid surface was used as a mask on UPEC channel to create seventh channel for calculating intra-organoid UPEC growth.

Serial block face scanning electron microscopy (SBEM) of co-culture of infected organoids with migrating neutrophils

tdTomato MBOs grown in ibidi µ-Dish were microinjected with UPEC. The UPEC was allowed to grow as biofilms within the lumen of organoids for 6 hours. After the two hours of bacterial growth within organoids, injected organoids were removed from fresh BME by pipetting 2 mL of ice cold Cell Recovery Solution after removing MBM from ibidi µ-Dish. The BME hydrogel was mechanically dissociated with a P1000 pipette and resulting liquid gel is placed inside 1% BSA pre-coated 15mL falcon tube. The ibidi µ-Dish was washed with additional 1.5 mL of Cell Recovery Solution twice to collect the organoids and, the resulting 5 mL of Cell Recovery Solution containing MBOs is occasionally mechanically dissociated with 1% BSA pre-coated non-tapered glass pipette. The cell recovery solution containing infected organoids is kept on ice for 30 minutes to completely liquify the BME. The cell recovery solution is washed twice with 10 mL of basal medium and the organoids are centrifuged at 0.1 g for 5 minutes at 4°C to remove the recovery solution. The microinjected tdTomato MBOs grown in ibidi µ-Dish were co-embedded with freshly isolated and CellTracker™ Deep Red labelled Ly6G neutrophils on a plasma treated MatTek dish with gridded coverslip. The organoids were fixed 6 hours after the MBM addition (supplemented with 25 ng/mL of mouse G-CSF). After 6 hours, organoids were fixed with a buffered mix of 1 % glutaraldehyde and 2 % paraformaldehyde in 0.1M phosphate buffer (pH 7.4) inside 15 mL falcon tube for 1 hour at room temperature. The infected organoid was fixed for one hour with the fixative, washed twice with PBS and then examined via optical microscopy to identify infected organoids with an IBC and neutrophils within the lumen,. The chosen organoid was then imaged on a confocal Leica Sp8 microscope using a low magnification 10X objective. The fluorescent image was acquired with 0.2 µm lateral and 1 µm axial resolution was used identify and locate it on the gridded coverslip for correlative light and SBEM. This fixed organoid was kept overnight at 4°C in the fixative.

The fixed organoids were then postfixed in potassium ferrocyanide (1.5%) and osmium (2%), then stained with thiocarbohydrazide (1%) followed by osmium tetroxide (2%) alone. They were finally stained overnight in uranyl acetate (1%), washed in distilled water at 50 °C before being stained with lead aspartate at a pH of 5.5 at the same temperature. The entire cover slip, with the organoids still attached, were then dehydrated in increasing concentrations of alcohol and then embedded in durcupan resin and hardened at 65 °C for 24 h. The total thickness of the coverslip and resin was minimized to around 1 mm. Once hardened, the coverslip was removed, and the region of resin, containing the organoid of interest, cut away from the others with a scalpel blade. This piece was glued, with conductive glue, to an aluminium holder, and then placed inside the scanning electron microscope (Merlin, Zeiss NTS) integrated with an in-chamber ultramicrotome device (3View, Gatan). Serial images, 100 nm part, were collected from the block face using a beam energy of 1.7 kV and 350 pA of current. Each image contained 6144 x 4608 pixels with a pixel size of 30 nm, and the stack contained 960 serial images. The overall volume imaged was 184.32 x 138.24 x 96 μm^3.

Labelling of bacteria, epithelial cells, neutrophils and organoid lumen from SBEM

Identification and labelling of different features (e.g. lumen boundary, neutrophils, bacteria) was done manually; features whose identity was doubtful were not included in the analysis. All the different bacterial categories were identified on the full stack (960 slices). We identified five different categories of bacteria: extracellular bacteria (in the organoid lumen), neutrophil bacteria (bacteria inside neutrophils), IBC bacteria (colony of intracellular bacterial community), intracellular bacteria (bacteria inside the epithelial cell cytoplasm) and pericellular bacteria

(bacteria between the cell boundaries). The injection site could be identified with asymmetry and higher abundance of extracellular lumenal bacteria towards one side of the lumen.

The IBC cell allowed x,y alignment of the fluorescent image with the SBEM stack. Boundary of the organoid lumen, organoid coverage, and neutrophil boundaries were marked on a reduced stack (480 z-stacks) with x,y,z pixel resolution (60nm, 60nm, 100nm). We also marked the location of epithelial cell nuclei. Fluorescent image of the cell tracker labelled neutrophils allowed identification and profiling of neutrophils. Neutrophils were identified with their multi-lobular nuclei with high electron density. 5 neutrophils were identified outside and 9 neutrophils were identified inside the organoid. After identifying the multi-lobular nuclei of the neutrophils, bacteria were found in the neutrophil cytoplasm.

3D analysis and modelling of the infected organoid

The serial electron micrographs were imported into the TrakEM2 software operating in FIJI. They were then aligned and the position of all cells and bacteria plotted in the image series. The lumen was also reconstructed by segmenting it in each of the images in which it appeared, as were the neutrophils, and the cells surrounding the IBC. For ease of manipulating the large dataset, the reconstruction of the lumen, neutrophils and position of the epithelial cells was done on a reduced stack of 480 slices with corresponding pixel size of 60 nm and spacing between subsequent slices of 200nm.

The segmentations of cells, the lumen, as well as the coordinates of each cell and bacteria, were exported to the Blender 3D modeling software. The ‘proximity tool’ in the NeuroMorph toolset

(Jorstad et al., 2018),was used to measure the distance of each bacteria to the wall of the lumen, as well as the organoid's surface. To visualize the organoid, with all bacteria, the particles system in the Blender software was used to place a single generic model of either a bacterium or a cell at the vertex that marked its 3D coordinate.

Scanning electron microscopy of infected organoids

UPEC-infected tdTomato MBOs were allowed to grow for 6 hours. After 6 hours, organoids were fixed with a buffered mix of 1 % glutaraldehyde and 2 % paraformaldehyde in 0.1 M phosphate buffer (pH 7.4) inside 15 mL falcon tube for 1 hour at room temperature. The fixed organoids were seeded onto a 12 mm poly-L-lysine-coated coverslips and kept overnight in the fixative. The organoids were further fixed with 1% osmium tetroxide in 0.1 M cacodylate buffer, and then dehydrated in increasing concentrations of ethanol starting at 50 % and 10 minutes for each incubation. Once in 100 % they finally underwent drying at the critical point of CO_2 (Leica CPD300) before being manipulated with a 0.125 mm tungsten needle (FST, 10130-05) using stereomicroscope (Leica M205) and adhered to aluminium stub using conductive tape (Election Microscopy Sciences, USA). This holder was then coated with 5 nm of gold palladium metal, using a sputter coater (Q150; Quorum Ltd, UK), and imaged in a scanning electron microscope (Merlin, Zeiss NTS).

References:

Andersen, T.E., Khandige, S., Madelung, M., Brewer, J., Kolmos, H.J., and Møller-Jensen, J. (2012). Escherichia coli uropathogenesis in vitro: invasion, cellular escape, and secondary infection analyzed in a human bladder cell infection model. Infect Immun *80*, 1858–1867.

Anderson, G.G., Palermo, J.J., Schilling, J.D., Roth, R., Heuser, J., and Hultgren, S.J. (2003). Intracellular Bacterial Biofilm-Like Pods in Urinary Tract Infections. Science *301*, 105–107.

Anderson, G.G., Dodson, K.W., Hooton, T.M., and Hultgren, S.J. (2004). Intracellular bacterial communities of uropathogenic Escherichia coli in urinary tract pathogenesis. Trends Microbiol *12*, 424–430.

Bartfeld, S., and Clevers, H. (2015). Organoids as Model for Infectious Diseases: Culture of Human and Murine Stomach Organoids and Microinjection of Helicobacter Pylori. J Vis Exp Jove.

Blango, M.G., Ott, E.M., Erman, A., Veranic, P., and Mulvey, M.A. (2014). Forced Resurgence and Targeting of Intracellular Uropathogenic Escherichia coli Reservoirs. Plos One *9*, e93327.

Cattan, V., Bernard, G., Rousseau, A., Bouhout, S., Chabaud, S., Auger, F.A., and Bolduc, S. (2011). Mechanical Stimuli-induced Urothelial Differentiation in a Human Tissue-engineered Tubular Genitourinary Graft. Eur Urol *60*, 1291–1298.

Chabaud, S., Saba, I., Baratange, C., Boiroux, B., Leclerc, M., Rousseau, A., Bouhout, S., and Bolduc, S. (2017). Urothelial cell expansion and differentiation are improved by exposure to hypoxia. J Tissue Eng Regen M *11*, 3090–3099.

Clevers, H. (2016). Modeling Development and Disease with Organoids. Cell *165*, 1586–1597.

Co, J.Y., Margalef-Català, M., Li, X., Mah, A.T., Kuo, C.J., Monack, D.M., and Amieva, M.R. (2019). Controlling Epithelial Polarity: A Human Enteroid Model for Host-Pathogen Interactions. Cell Reports *26*, 2509-2520.e4.

Denk, W., and Horstmann, H. (2004). Serial Block-Face Scanning Electron Microscopy to Reconstruct Three-Dimensional Tissue Nanostructure. Plos Biol *2*, e329.

Foxman, B. (2010). The epidemiology of urinary tract infection. Nat Rev Urol *7*, 653–660.

Foxman, B., Gillespie, B., Koopman, J., Zhang, L., Palin, K., Tallman, P., Marsh, J.V., Spear, S., Sobel, J.D., Marty, M.J., et al. (2000). Risk Factors for Second Urinary Tract Infection among College Women. Am J Epidemiol *151*, 1194–1205.

Hannan, T.J., and Hunstad, D.A. (2016). A Murine Model for Escherichia coli Urinary Tract Infection. Methods Mol Biology Clifton N J *1333*, 159–175.

Haraoka, M., Hang, L., Frendéus, B., Godaly, G., Burdick, M., Strieter, R., and Svanborg, C. (1999). Neutrophil Recruitment and Resistance to Urinary Tract Infection. J Infect Dis *180*, 1220–1229.

Heo, I., Dutta, D., Schaefer, D.A., Iakobachvili, N., Artegiani, B., Sachs, N., Boonekamp, K.E., Bowden, G., Hendrickx, A.P.A., Willems, R.J.L., et al. (2018). Modelling Cryptosporidium infection in human small intestinal and lung organoids. Nat Microbiol *3*, 814–823.

Hoffman, D.P., Shtengel, G., Xu, C.S., Campbell, K.R., Freeman, M., Wang, L., Milkie, D.E., Pasolli, H.A., Iyer, N., Bogovic, J.A., et al. (2020). Correlative three-dimensional super-resolution and block-face electron microscopy of whole vitreously frozen cells. Science *367*, eaaz5357.

Horsley, H., Dharmasena, D., Malone-Lee, J., and Rohn, J.L. (2018). A urine-dependent human urothelial organoid offers a potential alternative to rodent models of infection. Sci Rep-Uk *8*, 1238.

Hung, C.-S., Dodson, K.W., and Hultgren, S.J. (2009). A murine model of urinary tract infection. Nat Protoc *4*, 1230–1243.

Jorstad, A., Blanc, J., and Knott, G. (2018). NeuroMorph: A Software Toolset for 3D Analysis of Neurite Morphology and Connectivity. Front Neuroanat *12*, 59.

Justice, S.S., Hung, C., Theriot, J.A., Fletcher, D.A., Anderson, G.G., Footer, M.J., and Hultgren, S.J. (2004). Differentiation and developmental pathways of uropathogenic Escherichia coli in urinary tract pathogenesis. Proc National Acad Sci *101*, 1333–1338.

Justice, S.S., Hunstad, D.A., Seed, P.C., and Hultgren, S.J. (2006). Filamentation by Escherichia coli subverts innate defenses during urinary tract infection. Proc National Acad Sci *103*, 19884–19889.

Kienle, K., and Lämmermann, T. (2016). Neutrophil swarming: an essential process of the neutrophil tissue response. Immunol Rev *273*, 76–93.

Klein, R.D., and Hultgren, S.J. (2020). Urinary tract infections: microbial pathogenesis, host-pathogen interactions and new treatment strategies. Nat Rev Microbiol *18*, 211–226.

Lämmermann, T., Afonso, P.V., Angermann, B.R., Wang, J.M., Kastenmüller, W., Parent, C.A., and Germain, R.N. (2013). Neutrophil swarms require LTB4 and integrins at sites of cell death in vivo. Nature *498*, 371–375.

Lane, M.C., Alteri, C.J., Smith, S.N., and Mobley, H.L.T. (2007). Expression of flagella is coincident with uropathogenic Escherichia coli ascension to the upper urinary tract. Proc National Acad Sci *104*, 16669–16674.

Lee, S.H., Hu, W., Matulay, J.T., Silva, M.V., Owczarek, T.B., Kim, K., Chua, C.W., Barlow, L.J., Kandoth, C., Williams, A.B., et al. (2018). Tumor Evolution and Drug Response in Patient-Derived Organoid Models of Bladder Cancer. Cell *173*, 515-528.e17.

Liese, J., Rooijakkers, S.H.M., Strijp, J.A.G. van, Novick, R.P., and Dustin, M.L. (2012). Intravital two-photon microscopy of host-pathogen interactions in a mouse model of Staphylococcus aureus skin abscess formation: Intravital 2-P microscopy of S.□aureus skin infection. Cell Microbiol *15*, 891–909.

Liu, Y., Stein, E., Oliver, T., Li, Y., Brunken, W.J., Koch, M., Tessier-Lavigne, M., and Hogan, B.L.M. (2004). Novel Role for Netrins in Regulating Epithelial Behavior during Lung Branching Morphogenesis. Curr Biol *14*, 897–905.

Maclachlan, C., Sahlender, D.A., Hayashi, S., Molnár, Z., and Knott, G. (2018). Block Face Scanning Electron Microscopy of Fluorescently Labeled Axons Without Using Near Infra-Red Branding. Front Neuroanat *12*, 88.

Martinez, J.J., Mulvey, M.A., Schilling, J.D., Pinkner, J.S., and Hultgren, S.J. (2000). Type 1 pilus-mediated bacterial invasion of bladder epithelial cells. Embo J *19*, 2803–2812.

Mullenders, J., Jongh, E. de, Brousali, A., Roosen, M., Blom, J.P.A., Begthel, H., Korving, J., Jonges, T., Kranenburg, O., Meijer, R., et al. (2019). Mouse and human urothelial cancer organoids: A tool for bladder cancer research. Proc National Acad Sci *116*, 201803595.

Mulvey, M.A., Lopez-Boado, Y.S., Wilson, C.L., Roth, R., Parks, W.C., Heuser, J., and Hultgren, S.J. (1998). Induction and Evasion of Host Defenses by Type 1-Piliated Uropathogenic Escherichia coli. Science *282*, 1494–1497.

Mulvey, M.A., Schilling, J.D., Martinez, J.J., and Hultgren, S.J. (2000). Bad bugs and beleaguered bladders: Interplay between uropathogenic Escherichia coli and innate host defenses. Proc National Acad Sci *97*, 8829–8835.

Mulvey, M.A., Schilling, J.D., and Hultgren, S.J. (2001). Establishment of a Persistent Escherichia coli Reservoir during the Acute Phase of a Bladder Infection. Infect Immun *69*, 4572–4579.

Muzumdar, M.D., Tasic, B., Miyamichi, K., Li, L., and Luo, L. (2007). A global double□fluorescent Cre reporter mouse. Genesis *45*, 593–605.

Mysorekar, I.U., and Hultgren, S.J. (2006). Mechanisms of uropathogenic Escherichia coli persistence and eradication from the urinary tract. Proc National Acad Sci *103*, 14170–14175.

Neal, J.T., Li, X., Zhu, J., Giangarra, V., Grzeskowiak, C.L., Ju, J., Liu, I.H., Chiou, S.-H., Salahudeen, A.A., Smith, A.R., et al. (2018). Organoid Modeling of the Tumor Immune Microenvironment. Cell *175*, 1972-1988.e16.

Nikolaev, M., Mitrofanova, O., Broguiere, N., Geraldo, S., Dutta, D., Tabata, Y., Elci, B., Brandenberg, N., Kolotuev, I., Gjorevski, N., et al. (2020). Homeostatic mini-intestines through scaffold-guided organoid morphogenesis. Nature *585*, 574–578.

Qian, X., Nguyen, H.N., Jacob, F., Song, H., and Ming, G.-L. (2017). Using brain organoids to understand Zika virus-induced microcephaly. Dev Camb Engl *144*, 952–957.

Rossi, G., Manfrin, A., and Lutolf, M.P. (2018). Progress and potential in organoid research. Nat Rev Genet *19*, 671–687.

Sachs, N., Papaspyropoulos, A., Ommen, D.D.Z., Heo, I., Böttinger, L., Klay, D., Weeber, F., Huelsz□Prince, G., Iakobachvili, N., Amatngalim, G.D., et al. (2019). Long□term expanding human airway organoids for disease modeling. Embo J *38*.

Sanden, S.M.G. van der, Sachs, N., Koekkoek, S.M., Koen, G., Pajkrt, D., Clevers, H., and Wolthers, K.C. (2018). Enterovirus 71 infection of human airway organoids reveals VP1-145 as a viral infectivity determinant. Emerg Microbes Infec *7*, 84.

Schilling, J.D., Lorenz, R.G., and Hultgren, S.J. (2002). Effect of Trimethoprim-Sulfamethoxazole on Recurrent Bacteriuria and Bacterial Persistence in Mice Infected with Uropathogenic Escherichia coli. Infect Immun *70*, 7042–7049.

Scott, V.C.S., Haake, D.A., Churchill, B.M., Justice, S.S., and Kim, J.-H. (2015). Intracellular Bacterial Communities: A Potential Etiology for Chronic Lower Urinary Tract Symptoms. Urology *86*, 425–431.

Shannon, J.G., Hasenkrug, A.M., Dorward, D.W., Nair, V., Carmody, A.B., and Hinnebusch, B.J. (2013). Yersinia pestis Subverts the Dermal Neutrophil Response in a Mouse Model of Bubonic Plague. Mbio *4*, e00170-13.

Smith, Y.C., Grande, K.K., Rasmussen, S.B., and O'Brien, A.D. (2006). Novel Three-Dimensional Organoid Model for Evaluation of the Interaction of Uropathogenic Escherichia coli with Terminally Differentiated Human Urothelial Cells. Infect Immun *74*, 750–757.

Southgate, J., Hutton, K.A., Thomas, D.F., and Trejdosiewicz, L.K. (1994). Normal human urothelial cells in vitro: proliferation and induction of stratification. Laboratory Investigation J Technical Methods Pathology *71*, 583–594.

Suzuki, K., Koyanagi-Aoi, M., Uehara, K., Hinata, N., Fujisawa, M., and Aoi, T. (2019). Directed differentiation of human induced pluripotent stem cells into mature stratified bladder urothelium. Sci Rep-Uk *9*, 10506.

Wakamoto, Y., Dhar, N., Chait, R., Schneider, K., Signorino-Gelo, F., Leibler, S., and McKinney, J.D. (2013). Dynamic Persistence of Antibiotic-Stressed Mycobacteria. Science *339*, 91–95.

Williamson, I.A., Arnold, J.W., Samsa, L.A., Gaynor, L., DiSalvo, M., Cocchiaro, J.L., Carroll, I., Azcarate-Peril, A., Rawls, J.F., Allbritton, N.L., et al. (2018). A High-Throughput Organoid Microinjection Platform to Study Gastrointestinal Microbiota and Luminal Physiology. Cell Mol Gastroenterology Hepatology *6*, 301–319.

Wright, K.J., Seed, P.C., and Hultgren, S.J. (2007). Development of intracellular bacterial communities of uropathogenic Escherichia coli depends on type 1 pili. Cell Microbiol *9*, 2230–2241.

Yuki, K., Cheng, N., Nakano, M., and Kuo, C.J. (2020). Organoid Models of Tumor Immunology. Trends Immunol *41*, 652–664.

Zhou, J., Li, C., Sachs, N., Chiu, M.C., Wong, B.H.-Y., Chu, H., Poon, V.K.-M., Wang, D., Zhao, X., Wen, L., et al. (2018). Differentiated human airway organoids to assess infectivity of emerging influenza virus. P Natl Acad Sci Usa *115*, 6822–6827.